Chemical Engineering Journal 166 (2011) 240–248

Contents lists available at ScienceDirect

Chemical Engineering Journal

journal homepage: www.elsevier.com/locate/cej

Adaptive predictive collocation with a cubic spline interpolation function for convection-dominant fixed-bed processes: Application to a fixed-bed adsorption process

Wangyun Won, Kwang Soon Lee*

Department of Chemical and Biomolecular Engineering, Sogang University, 1-Shinsoodong, Mapogu, Seoul 121-742, Republic of Korea

ARTICLE INFO

Article history:
Received 2 August 2010
Received in revised form 25 October 2010
Accepted 26 October 2010

Keywords:
Adaptive collocation
Cubic spline collocation
Moving finite element method
Fixed-bed adsorption
Pressure swing adsorption

ABSTRACT

Interference effects and nonlinearities that are inherent in an adsorption equilibrium add challenges to the task of modeling fixed-bed adsorption processes. In particular, the interference effect tends to produce steep transient concentration fronts, which are enhanced by the high convection to dispersion ratio that is found in normal bed operation conditions. This causes spatial stiffness and renders numerical computations difficult and inaccurate. To solve this problem, we propose a novel numerical procedure using gradient-directed adaptive predictive collocation with a cubic spline interpolation function and far-side boundary conditions. The spatial domain is divided into fixed subdomains and the number of collocation points for each subdomain is adaptively adjusted according to the present location and advancement speed of the maximum gradient in each subdomain. The proposed method was applied to a fixed-bed adsorption process capturing CO_2 from a CO_2/N_2 gas mixture and its effectiveness was compared with that of cubic spline and orthogonal collocation methods with fixed interpolation points, respectively. The effects of kinetic rates on the simulation results were also investigated from the viewpoint of accuracy and CPU time.

1. Introduction

Pressure swing adsorption (PSA) has been employed for a variety of gas separation processes such as the separation of oxygen from air, hydrogen from reformate mixture, and paraffin from mixed hydrocarbons. PSA has also received attention as a potentially viable option for the capture of CO_2 from large CO_2-generating sources [1,2]. The operation of the PSA process involves a number of complicated steps, and numerical simulation studies have played a crucial role in finding new operating conditions that improve the feasibility of the process [3,4]. To this end, a numerical solution should be accurate and fast enough to replace or minimize experimental studies. The interference effect caused by competitive adsorption tends to produce steep concentration fronts; this situation is aggravated by the high convection to dispersion ratio found in normal bed operations. This may cause spatial stiffness and can render numerical computations inaccurate and burdensome.

To accurately solve such problems, either the entire bed or the region around the sharp profile front must be densely discretized. The former approach is mathematically simple and can be easily programmed, but the computational burden can become heavy. The latter method allows one to use fewer grid points but requires adaptive grid allocation for each integration step tracing the sharp profile fronts.

Adaptive grid allocation methods have been mostly studied in the framework of finite element methods (FEM) and can be classified into two groups depending on how the finite elements are manipulated during integration. The first group has a fixed number of elements and also has fixed number of grids in each element, but the size (or length for the one-dimensional case) of the elements varies during integration [5–9]. In this method, penalty functions are required to avoid the singularity problem caused by two closely neighboring nodes. In contrast, the second group, often called the local refinement method, adjusts the number of grids in each element, whereas the number and size of the elements are fixed [10,11]. The common methods used to approximate profiles within an element include finite difference [12], orthogonal collocation (OC) [6,10], and the method of characteristics [13,14]. Because of their capability to effectively handle the stiffness problem, FEMs with adaptive grid allocation have been

Abbreviations: APCSC, adaptive predictive cubic spline collocation; BC, boundary condition; CSC, cubic spline collocation; FEM, finite element method; FSBC, far-side boundary condition; GD, gradient-directed; LDF, linear driving force; OC, orthogonal collocation; ODE, ordinary differential equation; PDE, partial differential equation; PSA, pressure swing adsorption; RMSE, root mean squared error.

* Corresponding author. Tel.: +82 2 705 8477; fax: +82 2 3272 0319.
E-mail address: kslee@sogang.ac.kr (K.S. Lee).

1385-8947/$ – see front matter © 2010 Published by Elsevier B.V.
doi:10.1016/j.cej.2010.10.067

Nomenclature

b_i	Langmuir constant of component i, kPa
C	concentration in gas phase, mol/cm^3
C_i	concentration of component i in gas phase, mol/cm^3
c_g	specific heat of gas, J/g K
c_s	specific heat of adsorbent, J/g-ads. K
c_w	specific heat of bed wall, J/g K
D_{ax}	mass axial dispersion coefficient, cm^2/s
D_l	lth subdomain
D_m	molecular diffusivity of gas, cm^2/s
d_p	particle diameter, cm
ΔH_i	average isosteric heat of adsorption for component i, J/mol
h_I	internal heat transfer coefficient, J/cm^2 s K
h_o	external heat transfer coefficient, J/cm^2 s K
k_g	thermal conductivity of gas, J/cm s K
k_i	mass transfer coefficient of linear driving force model of component i, s
L	bed length, cm
L_{fs}	far-side boundary condition, cm
P	pressure, kPa
P_i	partial pressure of component i, y_iCRT, kPa
Pr	Prandtl number = $c_g\mu/k_g$
q_i	amount adsorbed of component i, mol/g-ads.
$q_{m,i}$	maximum amount adsorbed of component i, mol/g-ads.
q_i^*	equilibrium adsorbed phase concentration, mol/g-ads.
R	gas constant = 8314.395 kPa cm^3/mol K
Re	Reynolds number = $\rho_g\varepsilon u d_p/\mu$
r_{bI}	internal bed radius, cm
r_{bO}	external bed radius, cm
Sc	Schmidt number = $\mu/\rho_g D_m$
S_w	$S_w \triangleq \pi(r_{bo}^2 - r_{bI}^2)$
T	gas temperature, K
T_{amb}	ambient temperature, K
T_w	wall temperature of the bed, K
u	interstitial linear gas velocity, cm/s
y_i	mole fraction of component i
z	axial position

Greek letters

ε	bed porosity
λ_{ax}	effective axial thermal conductivity of gas, J/cm s K
ρ_g	gas density, g/cm^3
ρ_s	adsorbent density, g-ads./cm^3
ρ_w	bed wall density, g/cm^3
μ	gas viscosity, kPa s

used, but not widely yet, to simulate the fixed-bed adsorption process.

A new cubic spline collocation (CSC) method with adaptive grid allocation is proposed in this research as a numerical solution technique for the one-dimensional fixed-bed adsorption process. The idea for adaptive grid allocation is taken from Yu and Wang [10], but the details of the proposed method contain elaborations and improvements. The spatial domain is divided into fixed finite elements, and the number of collocation points in each element is determined according to the magnitude, location, and speed of the steep fronts within the element. In particular, the speed information is used to predict the movement of the steep fronts during the next integration interval and to pre-allocate the collocation points in the forward elements. The proposed method identically applies cubic spline conditions to both the nodal and the internal grid points of the finite elements; therefore, it does not belong to the FEM group and can be termed as a so-called gradient-directed adaptive predictive cubic spline collocation (GD-APCSC) method. An obvious advantage of the proposed method over OC-based methods is that undesirable ripples, frequently observed in OC-based methods with high-order polynomial interpolation functions, can be effectively suppressed. Another advantage is that the proposed method can reduce the number of collocation points compared to the existing adaptive grid allocation methods by utilizing the information of not only the present location but also the advancement speed of the steep front in the determination of grid allocation. An additional feature of the proposed method is that the so-called far-side boundary condition (FSBC) is taken into account in the process model. In the ordinary modeling of a fixed-bed adsorption process or similar convection–diffusion processes, a zero-gradient is assumed at the outlet position of the bed as a boundary condition, whereas the true zero-gradient holds only at an infinite point. The FSBC corresponds to the zero-gradient condition at a finite point far outside the spatial domain, which is a feasible approximation of the physically correct condition. The proposed APCSC method can adopt the FSBC without increasing complexity or programming difficulty.

The performance of the proposed technique was evaluated at different stages. First, the superiority of CSC to OC and the importance of the FSBC are demonstrated with a linear convection–diffusion problem with fixed collocation points. Then, a fixed-bed adsorption model is solved using the proposed APCSC, and the performance is compared with the fixed-point CSC and Yu and Wang's approach [10], respectively, in terms of accuracy and computation time. The numerical solution of the adsorption process is highly sensitive to kinetic parameters and the effects of LDF constants on the simulation results are also investigated.

2. Mathematical model with far-side boundary conditions

2.1. Mathematical model of an adsorption bed

A non-isothermal dynamic model of an adsorption bed is considered in this study. The major assumptions of the model include:

(i) The radial concentration and temperature distributions are negligible.
(ii) The adsorption equilibrium is represented by Langmuir isotherms.
(iii) The ideal gas law is applicable.
(iv) Thermal equilibrium between the adsorbent and bulk gas is assumed.
(v) The mass transfer rate is represented by the LDF model.

On the basis of the above assumptions, the overall mass balance is written as:

$$\frac{\partial C}{\partial t} + \frac{1-\varepsilon}{\varepsilon}\rho_s \sum_{j=1}^{2} \frac{\partial q_j}{\partial t} + \frac{1}{L}\frac{\partial (uC)}{\partial z} = 0 \quad (1)$$

The mass balance for component i in the bulk phase is given by:

$$\frac{\partial C_i}{\partial t} + \frac{1-\varepsilon}{\varepsilon}\rho_s \frac{\partial q_i}{\partial t} - \frac{D_{ax}}{L^2}\frac{\partial^2 C_i}{\partial z^2} + \frac{1}{L}\frac{\partial (uC_i)}{\partial z} = 0 \quad (2)$$

The enthalpy balance for the combined gas and solid phases is written as:

Table 1
Parameters of the adsorption process.

Dimension of the adsorption bed and characteristics of zeolite 13X	
L (cm) = 60	$\varepsilon = 0.334$
d_p (cm) = 0.25	D_m (cm^2/s) = 0.16
r_{bI} (cm) = 1.5	r_{bo} (cm) = 2.125
ρ_w (g/cm^3) = 7.98	ρ_s (g-ads./cm^3) = 1.17
c_w (J/g K) = 0.504	c_s (J/g-ads. K) = 0.924
Parameters of extended Langmuir isotherms and heats of adsorption [16]	
$q_{m,i} = w_{1,i}\exp(w_{2,i}T)$, $b_i = w_{3,i}\exp(w_{4,i}T)$	
w_{1,CO_2} (mol/g-ads.) = 0.01943	w_{1,N_2} (mol/g-ads.) = 0.007683
w_{2,CO_2} (K) = -4.638×10^{-3}	w_{2,N_2} (1/K) = -6.739×10^{-3}
w_{3,CO_2} (kPa) = 122.69	w_{3,N_2} (1/kPa) = 32.06
w_{4,CO_2} (K) = -23.522×10^{-3}	w_{4,N_2} (1/K) = -26.941×10^{-3}
$-\Delta H_{CO_2}$ (J/mol) = 34998.6	$-\Delta H_{N_2}$ (J/mol) = 24998.4
Supplementary equations	
$-\frac{\partial P}{\partial z} = 150.0\frac{(1-\varepsilon)^2}{\varepsilon^2}\frac{\mu}{d_p^2}u + 1.75\frac{1-\varepsilon}{\varepsilon}\frac{\rho_g}{d_p}u\lvert u\rvert$ in [19]	
$\frac{\varepsilon D_{ax}}{D_m} = 20 + 0.5Re\,Sc$ in [15]	
$\frac{\lambda_{ax}}{k_g} = 7 + 0.5Pr\,Re$ in [24]	
Heat transfer coefficients	
h_I (J/cm^2 s K) = 0.003864	h_o (J/cm^2 s K) = 0.001428

$$(\varepsilon\rho_g c_g + (1-\varepsilon)\rho_s c_s)\frac{\partial T}{\partial t} - (1-\varepsilon)\rho_s\sum_{j=1}^{2}(-\Delta H_j)\frac{\partial q_j}{\partial t} - \frac{\lambda_{ax}}{L^2}\frac{\partial^2 T}{\partial z^2} + \frac{\rho_g c_g}{L}\frac{\partial(uT)}{\partial z} + \frac{2h_I}{r_{bI}}(T - T_w) = 0 \quad (3)$$

All of the symbols are defined in Nomenclature section, and the parameter values are listed in Table 1. It is assumed that the physical properties of the mixture gas follow the quadratic mixing rule. The last term in Eq. (3) accounts for heat transfer to the column wall. Neglecting the distribution in the radial and axial directions, the column wall temperature is assumed to satisfy the following dynamic equation at each z-position:

$$\rho_w c_w S_w\frac{\partial T_w}{\partial t} = 2\pi r_{bI}h_I(T - T_w) - 2\pi r_{bo}h_o(T_w - T_{amb}) \quad (4)$$

Using the relation $C_i = C_{yi}$, where y_i denotes the mole fraction of component i, Eq. (2) can be restated as:

$$\frac{\partial y_i}{\partial t} = -\frac{1-\varepsilon}{C\varepsilon}\rho_s\frac{\partial q_i}{\partial t} + \frac{D_{ax}}{L^2 C}\left(C\frac{\partial^2 y_i}{\partial z^2} + 2\frac{\partial C}{\partial z}\frac{\partial y_i}{\partial z} + y_i\frac{\partial^2 C}{\partial z^2}\right) - \frac{u}{L}\frac{\partial y_i}{\partial z} + \frac{y_i(1-\varepsilon)}{C\varepsilon}\rho_s\sum_{j=1}^{N}\frac{\partial q_j}{\partial t} \quad (5)$$

In this study, we consider an adsorption process that captures CO_2 from a CO_2/N_2 gas mixture using zeolite 13X. The mass transfer for the concerned process is frequently expressed by the LDF approximation with a single lumped mass transfer coefficient, k_i, which is known as LDF constant [15]:

$$\frac{\partial q_i}{\partial t} = k_i(q_i^* - q_i) \quad (6)$$

where q_i^* represents the fictitious adsorbed phase concentration in equilibrium with the local bulk gas phase concentration for component i, and the adsorption equilibrium is known to be appropriately represented by the extended Langmuir isotherm equation [16]:

$$q_i^* = \frac{q_{m,i}b_i P_i}{1 + \sum_{i=1}^{2} b_i P_i} \quad (7)$$

The kinetic description may be improved if a more sophisticated kinetic model for energetically heterogeneous surface such as Elovich and second-order equations or a micro-pore diffusion model valid for zeolite-type adsorbents [17] is employed depending on the adsorbent type. Nonetheless, the LDF model is still widely employed for the case of CO_2 adsorption in zeolite [1,4,18]. The APCSC technique introduced in the subsequent sections need not be modified by the choice of a kinetic model.

In addition to the above equations, the relationship between the gas velocity and the pressure distribution within the bed is expressed by the Ergun equation [19] and the formulas for D_{ax} in Eq. (2) and λ_{ax} in Eq. (3) are given in Table 1 together with other parameters used in the simulation study.

For the adsorption step, the BCs for Eqs. (3) and (5) are normally given as

$$y_{CO_2}(t, z=0) = y_{CO_2}^{feed}, \quad \frac{\partial y_{CO_2}(t, z=1)}{\partial z} = 0 \quad (8)$$

$$T(t, z=0) = T^{feed}, \quad \frac{\partial T(t, z=1)}{\partial z} = 0 \quad (9)$$

The velocity and pressure at $z = 0$ and 1 are assigned as

$$u(t, z=0) = u^{feed}, \quad P(t, z=1) = 101.3 \ \text{kPa} \quad (10)$$

Initially, the bed is assumed to be filled with N_2, which can be described as

$$y_{CO_2}(0, z) = 0, \quad q_i(0, z) = q_{N_2}^*, \quad T(0, z) = T^{feed}, \quad P(0, z) = 101.3 \ \text{kPa} \quad (11)$$

where $q_{N_2}^*$ denotes the adsorbed phase concentration in equilibrium with pure N_2 at the temperature and pressure given in Eq. (11).

The above initial and boundary conditions are only for the adsorption step of the PSA process; different conditions are required for other steps such as pressurization, blow-down, and purge. According to the operating step, the steep front moves from $z = 0$ to $z = 1$ or in the reverse direction.

All of the dependent variables in the equations described above are normalized between 0 and 1 before reduction to ordinary differential equations using the collocation method.

2.2. Far-side boundary conditions

The BCs at $z = 1$ in Eqs. (8) and (9) are valid only when the column is sufficiently long, although they have been assumed as the BCs in many studies. In fact, the zero spatial derivative holds only for $z \to \infty$. To render a model physically more reasonable, the BCs in Eqs. (8) and (9) are replaced with the FSBC [20], which is an approximation of the zero slope condition at infinity at a finite distance:

$$0 = \left.\frac{\partial y_i(t, z)}{\partial z}\right|_{z\to\infty} \approx \frac{\partial y_i(t, z = z_{fs})}{\partial z}, \quad z_{fs} \gg 1 \quad (12)$$

where z_{fs} denotes the far-side point. In this paper, $z_{fs} = 5$ is assumed and found to be sufficiently large. Use of the FSBC in CSC is straightforward and results in only a minor increase in the order of the ODE model.

3. Adaptive predictive cubic spline collocation

The concentration and temperature profiles of the concerned system become steeper with decreasing D_{ax} and λ_{ax} and increasing k_i's. Real processes normally exhibit very steep profiles, and a correct simulation with fixed discretization requires a large number of grid points, resulting in a heavy computational burden. In this chapter, we describe a discretization technique proposed to cope with this problem.

In the proposed technique, the spatial domain is divided into a number of fixed subdomains, and the collocation points are allotted on each subdomain for each integration period in an adaptive manner using information on the maximum gradient. Once the collocation points are determined, the solution is found using the CSC method. This procedure can be described in greater detail as follows:

Step 1. Define the subdomain division and an appropriate number and locations of collocation points on the subdomain.
Step 2. Compute the matrices for CSC [in Eq. (17)] and construct an ODE model [in Eqs. (20)–(24)] using the CSC method.
Step 3. Integrate the ODE model from t to $t+\Delta t$.
Step 4. Update the number and location of collocation points for each subdomain for the next integration interval referring to the magnitude, location, and speed of the maximum gradient of the solution profiles at $t+\Delta t$.
Step 5. Integrate the ODE model over the next interval and repeat steps 2–5 until the terminal time is reached.

We now describe the details of the CSC method and the proposed adaptive collocation technique.

3.1. Cubic spline collocation method

The collocation method is an approximate solution technique for differential equations defined over a bounded spatial domain. Usually, a linear combination of a finite number of basis functions for the spatial domain is chosen as a trial function, or equivalently, an interpolation function, and the coefficients are determined so that the differential equation is satisfied by the interpolation function at pre-selected points known as collocation points. In OC, the roots of an Nth-order orthogonal polynomial are taken as internal collocation points, and an $N+1$th-order polynomial for the spatial variable is used as the interpolation function. In CSC, on the other hand, the cubic spline is used for the interpolation function, with no special rule to define the collocation points. The cubic spline is inherently smoother than high-order polynomials, and ripples that are frequently observed in the OC solution of a stiff problem can be effectively suppressed [21,22].

A cubic spline with interpolation points at z_0 (=0), $z_1, \ldots, z_N$ (=1) can be represented as a concatenation of cubic polynomials defined over each interval $[z_k, z_{k+1}]$, $k=0, \ldots, N-1$, such that

$$w(z) = \sum_{k=0}^{N-1} p_k(z) v_k(z) \tag{13}$$

where $v_k(z)$ is a piecewise constant function satisfying

$$v_k(z) = \begin{bmatrix} 1 & \text{for} \quad z \in [z_k, z_{k+1}) \\ 0 & \text{otherwise} \end{bmatrix} \tag{14}$$

and $p_k(z)$ denotes a cubic polynomial for the kth interval that satisfies the spline conditions and the natural cubic spline conditions

$$p_k^{(n)}(z_{k+1}) = p_{k+1}^{(n)}(z_{k+1}) \quad \text{for} \quad k = 0, \ldots, N-2, \quad n = 0,\ 1,\ 2 \tag{15a}$$

$$p_0^{(2)}(z_0) = p_{N-1}^{(2)}(z_N) = 0 \tag{15b}$$

where the superscript (n) denotes the nth-order spatial derivative. After some straightforward manipulations, the interpolation function in Eq. (13) can be rewritten as

$$w(z) = \mathbf{m}(z)^T \mathbf{w} \tag{16}$$

where $\mathbf{m}(z)$ is an $(N+1)\times 1$ vector function of z, and $w \triangleq \begin{bmatrix} w(z_0) & \cdots & w(z_{N-1}) & w(z_N) \end{bmatrix}^T = \begin{bmatrix} p_0(z_0) & \cdots & p_{N-1}(z_{N-1}) & p_{N-1}(z_N) \end{bmatrix}^T$. Using Eq. (16), we have

$$\frac{\partial \mathbf{w}}{\partial z} = \begin{bmatrix} \dfrac{\partial \mathbf{m}(z_0)^T}{\partial z} \\ \vdots \\ \dfrac{\partial \mathbf{m}(z_N)^T}{\partial z} \end{bmatrix} \mathbf{w} \triangleq \mathbf{A}\mathbf{w} \quad \text{and}$$

$$\frac{\partial^2 \mathbf{w}}{\partial z^2} = \begin{bmatrix} \dfrac{\partial^2 \mathbf{m}(z_0)^T}{\partial z^2} \\ \vdots \\ \dfrac{\partial^2 \mathbf{m}(z_N)^T}{\partial z^2} \end{bmatrix} \mathbf{w} \triangleq \mathbf{B}\mathbf{w} \tag{17}$$

Once the matrices corresponding to the spatial derivatives are available, reduction of the PDE's to a set of ODE's is rather straightforward. For this, let us define

$$\bar{y}_i \triangleq \begin{bmatrix} y_i(z_0) & \cdots & y_i(z_N) \end{bmatrix}^T \quad \text{and} \quad y_i \triangleq \begin{bmatrix} y_i(z_1) & \cdots & y_i(z_{N-1}) \end{bmatrix}^T \tag{18}$$

with similar expressions for $\mathbf{C}$, $\bar{\mathbf{C}}$, $\mathbf{T}$, $\bar{\mathbf{T}}$, $\mathbf{q}_i$, and $\bar{\mathbf{q}}_i$. If we eliminate the time derivative of q_j in Eq. (5) using Eq. (6), write the equation at the collocation points, z_0 to z_N, and employ the relationships in Eq. (17), we have

$$\frac{d\bar{y}_i}{dt} = \bar{\mathbf{F}}_y(\bar{\mathbf{C}}, \bar{\mathbf{T}}, \bar{\mathbf{q}}_j)\bar{\mathbf{y}}_i + \bar{\mathbf{H}}_y(\bar{\mathbf{C}}, \bar{\mathbf{T}}, \bar{\mathbf{q}}_j) \tag{19}$$

Note that the ODE is valid only at the internal collocation points, z_1 to z_{N-1} and that the BC's should hold at z_0 and z_N. Consequently, Eq. (19) is recast to:

$$\frac{dy_i}{dt} = \mathbf{F}_y(\mathbf{C}, \mathbf{T}, \mathbf{q}_j)\mathbf{y}_i + \mathbf{G}_y(\mathbf{C}, \mathbf{T}, \mathbf{q}_j)y_i(0) + \mathbf{H}_y(\mathbf{C}, \mathbf{T}, \mathbf{q}_j) \tag{20}$$

Eqs. (1) and (3) are reduced to sets of ODE's through the same procedure:

$$\frac{d\mathbf{T}}{dt} = \mathbf{F}_T(\mathbf{C}, \mathbf{y}_i, \mathbf{q}_j)\mathbf{T} + \mathbf{G}_T(\mathbf{C}, \mathbf{y}_i, \mathbf{q}_j)T(0) + \mathbf{Q}_T(\mathbf{C}, \mathbf{y}_i, \mathbf{q}_j) \tag{21}$$

$$\frac{d\mathbf{C}}{dt} = \mathbf{F}_C(\mathbf{T}, \mathbf{y}_i, \mathbf{q}_j)\mathbf{T} + \mathbf{G}_C(\mathbf{T}, \mathbf{y}_i, \mathbf{q}_j)C(0) + \mathbf{Q}_C(\mathbf{T}, \mathbf{y}_i, \mathbf{q}_j) \tag{22}$$

Finally, Eqs. (4) and (6) hold at each collocation point and this results in

$$\frac{d\boldsymbol{q}_i}{dt} = \boldsymbol{K}(\boldsymbol{T}, \boldsymbol{C}, \boldsymbol{y}_i, \boldsymbol{q}_j) \tag{23}$$

$$\frac{d\boldsymbol{T}_w}{dt} = \boldsymbol{H}(\boldsymbol{T}, \boldsymbol{T}_w, T_{amb}) \tag{24}$$

Eqs. (20)–(24) constitute the entire set of ODE's for the studied adsorption process.

3.2. Gradient-directed adaptive predictive allocation of the collocation points

The proposed gradient-directed adaptive predictive collocation method is an amelioration of the gradient-directed moving finite element technique of Yu and Wang [10]. Fig. 1 illustrates how the number of collocation points is adjusted in the proposed method. The z-domain [0, 1], is divided into fixed subdomains, and the number of collocation points for each subdomain for next integration interval $[t, t+\Delta t]$ is determined adaptively according to the following strategy: first, the profile of the maximum absolute gradient of the process variables for the lth-subdomain is estimated such that

$$g_l(t,z) \triangleq \max\left(\left|\frac{\partial y_{CO_2}(t,z)}{\partial z}\right|, \left|\frac{\partial y_{N_2}(t,z)}{\partial z}\right|, \left|\frac{\partial \hat{C}(t,z)}{\partial z}\right|, \left|\frac{\partial \hat{T}(t,z)}{\partial z}\right| \right) \tag{25}$$

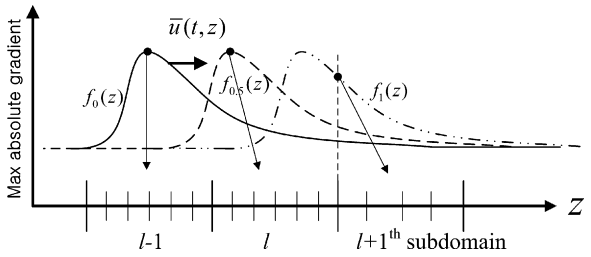

Fig. 1. Prediction of the maximum absolute gradient profiles and determination of the collocation points at t.

Note that the model equations are written with normalized dependent variables and that $\hat{C}$ and $\hat{T}$ represent the normalized concentration and temperature, respectively. In this study, $g_l(t,z)$ is obtained only at the present collocation points of the lth-subdomain. Next, by assuming that the profiles shift in the z-direction at the present sharp front speed, $\bar{u}(t,z)$, and assuming that the integration interval Δt is given such that the shift distance during Δt is less than two times the subdomain length, we estimate the shifted profile of $g_l(t,z)$ at the half time and at the end of the next integration interval as follows:

$$g_l(t+0.5\Delta t, z) = g_l(t, z-\alpha\bar{u}(t,z)(0.5\Delta t))$$
$$g_l(t+\Delta t, z) = g_l(t, z-\alpha\bar{u}(t,z)\Delta t) \quad (26)$$

The sharp front speed for the case of Langmuir isotherm can be computed using the equation developed by Suh and Wankat [23]:

$$\bar{u} = \frac{(1+\gamma y_{CO_2,b})(1+\gamma y_{CO_2,a})u}{\psi_{CO_2}\xi_{N_2} + (1+\gamma y_{CO_2,b})(1+\gamma y_{CO_2,a}) - [\psi_{CO_2}\xi_{N_2} - \psi_{N_2}\xi_{N_2}(1+\gamma)]y_{CO_2,a}} \quad (27)$$

where

$$\psi_i = q_{m,i}b_i\left(\frac{1-\varepsilon}{\varepsilon}\right)\rho_s RT, \quad \xi_i = \frac{1}{1+b_iP}, \quad \gamma = \frac{\xi_{N_2}}{\xi_{CO_2}} - 1,$$
$$i = CO_2, N_2 \quad (28)$$

and subscripts b and a refer to the quantity before and after the sharp front, respectively. The constant α in Eq. (26) defines a safety margin to compensate for a potential error of Eq. (27) and is given as 1.2 in this research. By concatenating $g_l(t,z)$, $g_l(t+0.5\Delta t,z)$, and $g_l(t+\Delta t,z)$ over l, the entire profiles of the absolute maximum gradient can be estimated before, mid-time, and after an integration interval, which are denoted as $f_0(z)$, $f_{0.5}(z)$, and $f_1(z)$, respectively. The number of collocation points for the lth subdomain, n_l, is determined using the maximum tangent angle defined by

$$\theta_l \triangleq \tan^{-1}\left(\max_{w\in\{0,0.5,1\}, z\in D_l} f_w(z)\right) \quad (29)$$

such that

$$\theta^0 = 0 \le \theta_l < \theta^1 \Rightarrow n_l = n^0 = 0 \quad (30a)$$
$$\theta^1 \le \theta_l < \theta^2 \Rightarrow n_l = n^{1\pi} \quad (30b)$$
$$\vdots$$
$$\theta^M \le \theta_l < \theta^{M+1} = \frac{\pi}{2} \Rightarrow n_l = n^M \quad (30c)$$

where θ^x and n^x are tuning factors.

The idea behind the above adaptation policy is clear; we predict the profile of the maximum absolute gradient value in each subdomain over the next integration period and allocate the necessary number of collocation points on each subdomain. If $f_{0.5}(z)$ and $f_1(z)$ are predicted as in Fig. 1, the number of collocation points for each subdomain is determined by the maximum value of the three overlapped profiles of $f(z)$, denoted by black circles. If Δt is short enough, it is not necessary to estimate $f_{0.5}(z)$. However, $f_1(z)$ should be estimated no matter how small Δt is because there is a possibility that a steep front exists near a subdomain boundary and intrudes into the next subdomain over a short time. In the reverse case, it is necessary to predict intermittent profiles on more subdomains ahead.

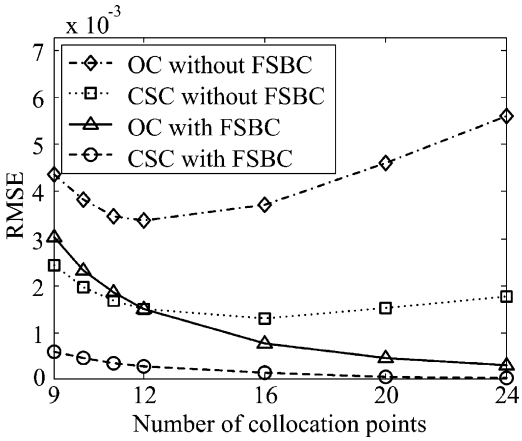

Fig. 2. Root mean squared errors of the solutions to Eq. (31) by OC and CSC without the FSBC, and OC and CSC with the FSBC when $P_e = 90$ and $\sigma = 30$.

4. Numerical results and discussion

The proposed method was evaluated under different perspectives. First, the performance of CSC and the necessity of the FSBC were demonstrated using a linear convection–diffusion problem with a known analytic solution. OC with the FSBC and CSC without the FSBC were also compared. Next, the accuracy and the computation time of the proposed method were compared with those of the fixed-grid CSC and Yu and Wang's approach [10] for an adsorption process. The effects of the LDF constants on the simulation results were also investigated. All of the numerical results were obtained using an Intel Core i7 CPU at 2.8 GHz, and the ODE models were integrated using the ode15s m-file in MATLAB.

4.1. Performance comparison of cubic spline collocation with orthogonal collocation and the importance of far-side boundary conditions

We first consider a linear convection–diffusion problem:

$$\frac{\partial^2 x}{\partial z^2} - P_e\frac{\partial x}{\partial z} - \sigma x = 0, \quad z\in(0,1] \quad \text{with} \quad x(0) = 1,$$
$$\left.\frac{\partial x}{\partial z}\right|_{z\to\infty} = 0 \quad (31)$$

where P_e represents the Peclet number. The solution becomes stiffer as P_e increases. The analytic solution is given as

$$x(z) = \exp\left(\frac{(P_e - \sqrt{P_e^2+4\sigma})z}{2}\right) \quad (32)$$

Numerical solutions were obtained for the above problem using OC and CSC with and without the FSBC, respectively, by increasing the number of collocation points. For the FSBC, z_{fs} is given as 5. The collocation points are given as the roots of the Legendre polynomial in OC and as equidistant points in CSC, respectively. Adaptive collocation was not considered in this problem. We assumed $P_e = 90$ and $\sigma = 30$ and the results are compared in Fig. 2 in terms of the root mean squared error (RMSE). It can be seen that CSC with the FSBC outperformed the other numerical methods in all cases. Note that the RMSE's from the OC and CSC with the FSBC decreased monotonically, whereas those with traditional BC's decreased and then

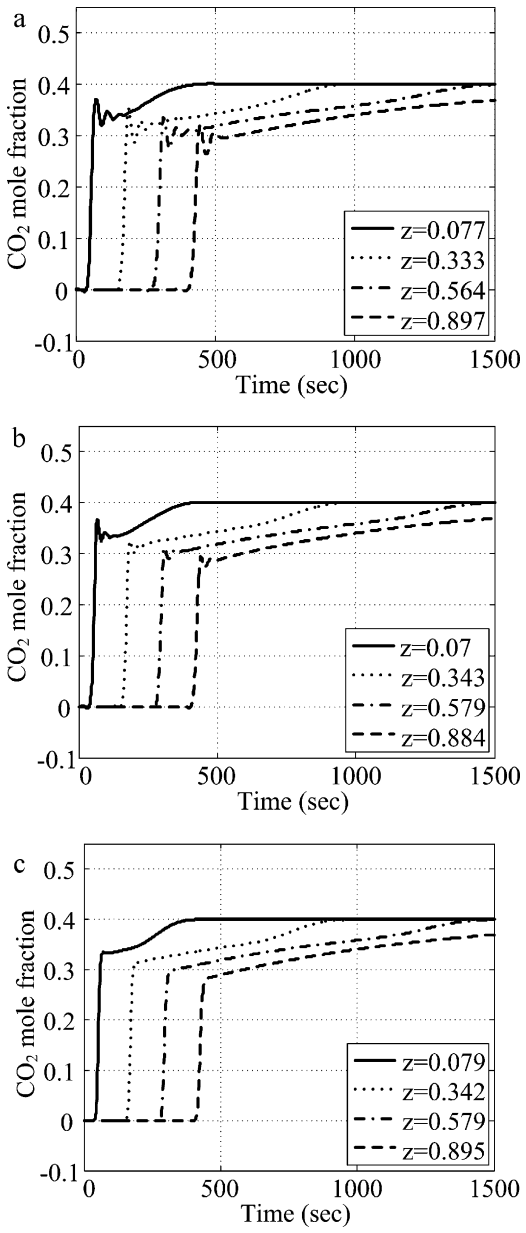

Fig. 3. Transient responses of CO_2 mole fraction: (a) CSC without the FSBC, (b) OC with the FSBC, and (c) CSC with the FSBC.

increased as the number of collocation points increased. All of these results indicate the necessity and importance of the FSBC. Fig. 2 also shows that CSC resulted in a smaller RMSE than OC for a given number of collocation points.

Next, CSC without the FSBC and OC and CSC with the FSBC were applied to the adsorption process as described in Section 2, with the parameter values given in Table 1. We assumed that the column was initially pre-saturated with pure N_2, and $y_{CO_2}^{feed} = 0.4$, $T^{feed} = 298.15$ K, and $u^{feed} = 35$ cm/s were implemented stepwise from $t = 0$. The number of collocation points was fixed at 49, and $z_{fs} = 5$ was assumed in all calculations. Fig. 3 shows the time-dependent profiles of y_{CO_2} at four selected z-positions. As the feed mixture was introduced at the bed inlet, a sharp concentration wave formed and moved toward the bed end as the feed mixture displaced N_2 in the adsorbed and bulk phases. Unrealistic ripples were produced around the wave fronts for CSC with traditional BCs and for OC with the FSBC. On the other hand, physically reasonable and smooth profiles with no such ripples were produced with CSC with the FSBC.

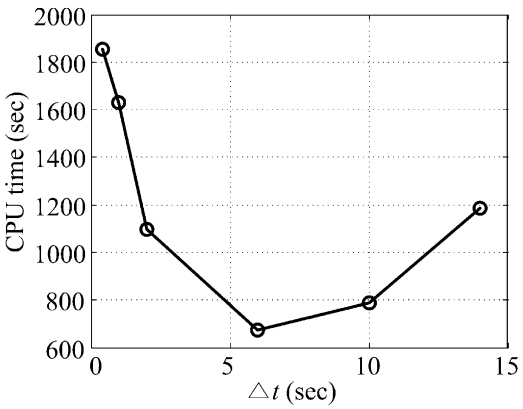

Fig. 4. CPU time depending on integration interval Δt.

4.2. Effects of the update period of collocation points

The number and location of the collocation points for each subdomain were updated periodically for each integration interval. To find the optimal update period of collocation points, the required CPU time was investigated for various integration intervals for the adsorption process with $y_{CO_2}^{feed} = 0.5$, $T^{feed} = 298.15$ K, $u^{feed} = 6.2$ cm/s, and $[k_{CO_2}, k_{N_2}] = [0.2, 1]$. The total integration time was 4000 s, and the associated APCSC tuning parameters are given as tuning policy 1 in Table 2. Fig. 4 shows that an optimal integration interval exists at around $\Delta t = 6$ s. When $\Delta t > 6$, the CPU time increased with an increasing number of subdomains in which the collocation points are densely allotted. In the case of $\Delta t < 6$, the CPU time increased sharply with decreasing Δt, caused by the increased frequency of the derivative call by the integrator. In Fig. 5, the CO_2 mole fraction profiles at four time points and the corresponding number and location of collocation points are presented for the case of $\Delta t = 6$ s and the total number of subdomain of 20. The collocation points were concentrated in the subdomain in which the sharp front was detected and in additional subdomains (marked by a shaded rectangle) through which the sharp front was expected to pass or reach during the next integration interval.

Table 2
APCSC tunings used.

Tuning policy	n^x, $x = 1, \ldots, M$ in Eq. (30)	θ^x, $x = 1, \ldots, M+1$ in Eq. (30)	Length of a sub-domain	Related figures and tables
1	0, 3, 7	0, 0.02, 0.04, $\pi/2$	0.05	Figs. 4 and 5
2	0, 6	0, 0.03, $\pi/2$	0.125	Case 5 in Table 3
3	0, 3, 6	0, 0.025, 0.05, $\pi/2$	0.0625	Case 6 in Table 3
4	0, 2, 3	0, 0.02, 0.04, $\pi/2$	0.125	Fig. 8(a)
5	0, 1, 2, 3	0, 0.02, 0.04, 0.06, $\pi/2$	0.1	Case 1 in Fig. 8(b)
6	0, 1, 2, 3	0, 0.02, 0.04, 0.06, $\pi/2$	0.0833	Case 2 in Fig. 8(b)
7	0, 1, 2, 3, 4	0, 0.01, 0.03, 0.06, 0.1, $\pi/2$	0.0667	Case 3 in Fig. 8(b)
8	0, 1, 2, 3, 4	0, 0.01, 0.03, 0.06, 0.1, $\pi/2$	0.05	Case 4 in Fig. 8(b)

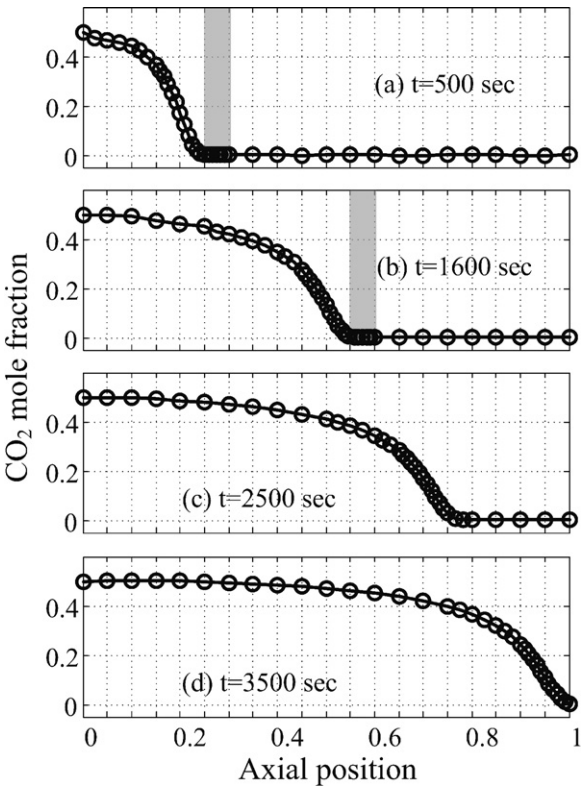

Fig. 5. Profiles of CO_2 mole fraction (solid lines) and the associated collocation points (circles) when the tuning policy 1 in Table 2 with $\Delta t = 6$ is applied: (a) $t = 500$ s, (b) $t = 1600$ s, (c) $t = 2500$ s, and (d) $t = 3500$ s. Boundaries of subdomains are indicated by dotted lines and the subdomains in which the steep front is expected to pass during the next integration interval is represented by shaded rectangles.

Fig. 6 compares snapshot profiles of CO_2 mole fractions obtained with the proposed APCSC method and with the moving finite element method of Yu and Wang [10] for the same adsorption process. For both methods, Δt was set at 10 s. Because the method of Yu and Wang [10] determines the number of collocation points based on the maximum gradient only at the present time and does not forecast its movement for the next integration interval, severe numerical errors occurred, as demonstrated in the figure.

4.3. Performance comparison between the fixed-grid cubic spline collocation method and the proposed adaptive collocation method

The performance of the proposed APCSC method was compared with that of the fixed-grid CSC technique in view of the CPU time and the accuracy of the solution for an adsorption process with $y_{CO_2}^{feed} = 0.6$, $T^{feed} = 298.15$ K, $u^{feed} = 15.4$ cm/s, and $[k_{CO_2}, k_{N_2}] = [0.2, 1]$. The total integration time for the simulation was chosen as 1500 s. The results are summarized in Table 3. A solution with 161 fixed collocation points was used as a reference, and the accuracy of the other solutions is presented in terms of the time- and space-averaged RMSE defined as

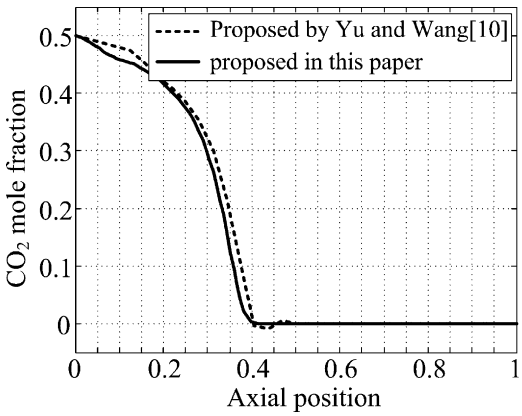

Fig. 6. Profiles of CO_2 mole fraction at $t = 1000$ s obtained with the proposed adaptive predictive grid method and the moving finite element method of Yu and Wang [10], respectively.

$$\text{RMSE} = \sqrt{\frac{1}{15 \times 8} \sum_{z=z_1}^{z_8} \sum_{t=t_1}^{t_{15}} (\hat{y}_{CO_2}(t,z) - \bar{y}_{CO_2}(t,z))^2} \qquad (33)$$

where z_i and t_i are 8 and 15 equally spaced points over the respective domains, and $\bar{y}_{CO_2}$ and $\hat{y}_{CO_2}$ represent the CO_2 mole fraction from the reference case and the other case under investigation, respectively. Cases 5 and 6 for APCSC were tuned according to tuning policies 2 and 3 in Table 2, respectively.

Cases 1 and 5 had similar numbers of collocation points and showed similar values for the CPU time. However, the RMSE was five times smaller for Case 5 (APCSC) than for Case 1 (fixed-grid CSC). Cases 2 and 6 showed similar RMSE values, but the number of collocation points and the required CPU time for Case 2 (fixed-grid CSC) were roughly two and eight times larger than those of Case 6 (APCSC), respectively. All of these results verify that the APCSC method efficiently utilized the collocation points and remarkably diminished the number of ODEs needed to solve the problem as compared to the fixed-grid method for a given solution accuracy.

4.4. Effects of kinetic constants

Among the various model parameters of the adsorption process, the kinetic constants, which correspond to the LDF constants in this study, have the most critical effects on the profiles of the process variables. As the rate of adsorption/desorption increases, the concentration and temperature profiles become steeper and results in the problem of spatial stiffness. In this section, the performance of the proposed APCSC method is evaluated for adsorption processes with different values of LDF constants.

Fig. 7 shows the profiles of the CO_2 mole fraction and bed temperature for $y_{CO_2}^{feed} = 0.4$, $T^{feed} = 298.15$ K, and $u^{feed} = 38.5$ cm/s obtained at $t = 150$ and 750 s, respectively, for three cases of LDF constants, $[k_{CO_2}, k_{N_2}] = [0.02, 0.1]$, $[0.05, 0.25]$, and $[0.3, 1.5]$. The total integra-

Table 3
Results of simulation study with the fixed-grid CSC and APCSC techniques.

Case	Method	Number of collocation points	Time- and space-averaged RMSE in Eq. (33)	CPU time (s)
1	Fixed-grid CSC	33	2.91×10^{-3}	125
2		73	2.66×10^{-4}	1602
3		121	2.29×10^{-4}	3677
4		161[a]	0	6897
5	APCSC	32 (time averaged)	6.08×10^{-4}	132
6		39 (time averaged)	2.73×10^{-4}	188

[a] Indicates the reference case to estimate RMSE values in other cases.

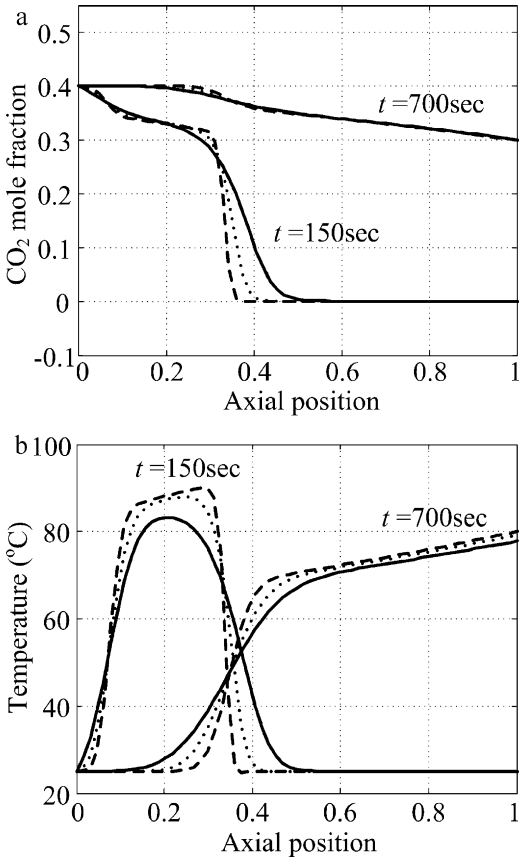

Fig. 7. Profiles of CO_2 mole fraction and bed temperature at $t = 150$ and 700 s, where solid, dotted, and dashed lines correspond to the cases of $[k_{CO_2}, k_{N_2}] = [0.02, 0.1]$, $[0.05, 0.25]$, and $[0.3, 1.5]$, respectively.

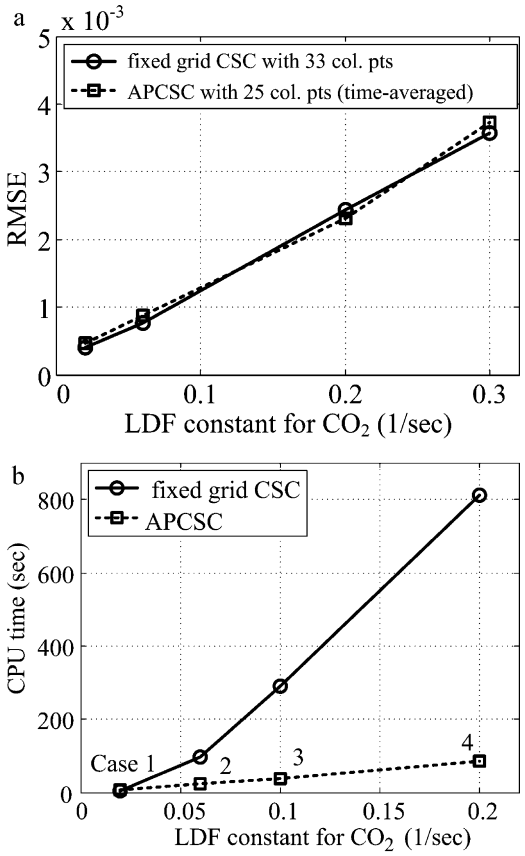

Fig. 8. Effects of LDF constants on the accuracy and CPU time when the fixed grid CSC and APCSC were applied to the adsorption process: (a) time and space averaged RMSE when the number of collocation points is constant and (b) CPU time when the RMSE was maintained constant for each method.

tion time was chosen as 2000 s. As we anticipated, the profiles became steeper as the LDF constants increased. Such steep profiles may cause oscillatory solutions when the number of collocation points is not sufficiently large.

Fig. 8 compares the performances of APCSC and fixed-grid CSC in view of the RMSE and CPU time for different LDF constants. The LDF constant for N_2 was assumed to be five times larger than that of CO_2. Fig. 8(a) compares the RMSE values from APCSC with tuning policy 4 in Table 2 and fixed-grid CSC applied to the adsorption process with four different LDF constants. The shortest distance between two adjacent collocation points with tuning policy 4 is 0.03125 (=0.125/(3 + 1)), and therefore, 33 (=1/0.03125 + 1) internal collocation points including $z = 1$ were assigned in the fixed-grid CSC method. In the APCSC approach, 25 collocation points were found to be used on average. The CPU times remained nearly constant, independent of the LDF constants, and were estimated to be around 100 and 60 s for the fixed-grid CSC and APCSC techniques, respectively. Because both methods share the same shortest collocation distance, the RMSE's appeared to be virtually the same for the given LDF constants.

The CPU times for varying numbers of collocation points (or tuning policies) that give a constant RMSE are plotted in Fig. 8(b). In all of the simulation cases, the RMSE was maintained around 4.0×10^{-4}. For this, the number of collocation points was chosen as 33, 39, 47, and 65 for the fixed-grid CSC and the tuning policies 5–8 in Table 2 were found to be appropriate for APCSC for the four LDF constants, respectively. Fig. 8(b) shows that the CPU time sharply increased with an increase in the LDF constant for the fixed-grid method due to the large number of unnecessary collocation points employed, which were assigned in flat regions. On the other hand, the CPU time increase was much smaller for APCSC. For the case in which $[k_{CO_2}, k_{N_2}] = [0.2, 1.0]$, the adaptive method required only one-tenth of the CPU time required when using the fixed-grid method. The purpose of APCSC is to reduce the computation burden by assigning more collocation points only on steep regions. Therefore, the flat region can have few collocation points, regardless of the increase in the total number of collocation points for steep profiles. The range of the steep region became narrower as the LDF constants increased, and the total number of collocation points could be further reduced if we were to use shorter subdomains and more frequently update the collocation points.

5. Conclusions

A novel adaptive predictive cubic spline collocation (APCSC) method with far-side boundary conditions (FSBC) was proposed to simulate stiff PDE systems such as PSA and simulated moving bed processes in which sharp moving wave fronts can develop. The proposed method is unique in that the prediction of the wave front location during the next integration interval is considered along with the present wave front location in the adaptive allotment of collocation points; adaptive collocation was applied to CSC; the PSA model was elaborated using the FSBC. All of these features make the proposed method novel and allow it to outperform the existing fixed-grid-based methods and the widely recognized moving finite element method of Yu and Wang [10] in terms of accuracy and computation time. Its performance was verified through numerical studies under various cases with a fixed-bed adsorption process model. We believe that the proposed APCSC method can

be employed as an effective tool for the analysis and synthesis of convection-dominant fixed-bed processes.

Acknowledgements

This work was supported by the Human Resources Development of the Korea Institute of Energy Technology Evaluation and Planning (KETEP) grant funded by the Korea government Ministry of Knowledge Economy (No. 20094010100160). K.S. Lee would like to acknowledge the financial support from NRF grant funded by the MEST through Mid-career Researcher Program (No. 2010-0000495). W. Won would like to appreciate Prof. Suh in the Department of Chemical Engineering at Hongik University, Seoul, Korea for his valuable technical assistance.

References

[1] J.H. Park, H.T. Beum, J.N. Kim, S.H. Cho, Numerical analysis on the power consumption of the PSA process for recovering CO_2 from flue gas, Ind. Eng. Chem. Res. 41 (2002) 4122–4131.
[2] M.T. Ho, G.W. Allinson, D.E. Wiley, Reducing the cost of CO_2 capture from flue gases using pressure swing adsorption, Ind. Eng. Chem. Res. 47 (2008) 4883–4890.
[3] S.P. Knaebel, D. Ko, L.T. Biegler, Simulation and optimization of a pressure swing adsorption system: recovering hydrogen from methane, Adsorption 11 (2005) 615–620.
[4] D. Ko, R. Siriwardane, L.T. Biegler, Optimization of a pressure-swing adsorption process using zeolite 13X for CO_2 sequestration, Ind. Eng. Chem. Res. 42 (2003) 339–348.
[5] M.C. Coimbra, C. Sereno, A. Rodrigues, Applications of a moving finite element method, Chem. Eng. J. 84 (2001) 23–29.
[6] K. Kaczmarski, M. Mazzotti, G. Storti, M. Morbidelli, Modeling fixed-bed adsorption columns through orthogonal collocations on moving finite elements, Comput. Chem. Eng. 21 (1997) 641–660.
[7] W.C. Huang, C.T. Chou, A moving finite element simulation of a pressure swing adsorption process, Comput. Chem. Eng. 21 (1997) 301–315.
[8] C. Sereno, A. Rodrigues, J. Villadsen, Solution of partial differential equations system by the moving finite element method, Comput. Chem. Eng. 16 (1992) 583–592.
[9] N.N. Carlson, K. Miller, Design and application of a gradient-weighted moving finite element code, SIAM J. Sci. Comput. 19 (1998) 728–798.
[10] Q. Yu, N.H.L. Wang, Computer simulations of the dynamics of multicomponent ion exchange and adsorption in fixed beds – gradient-directed moving finite element method, Comput. Chem. Eng. 13 (1989) 915–926.
[11] I. Babuska, J. Chandra, J.E. Flaherty, Adaptive Computational Method for Partial Differential Equations, Society for Industrial and Applied Mathematics, Philadelphia, 1983.
[12] S.J. Doong, R.T. Yang, Bulk separation of multicomponent gas mixtures by pressure swing adsorption: pre/surface diffusion and equilibrium models, AIChE J. 32 (1986) 397–410.
[13] J.C. Kayser, K.S. Knaebel, Pressure swing adsorption: development of an equilibrium theory for binary gas mixtures with nonlinear isotherm, Chem. Eng. Sci. 44 (1989) 1–8.
[14] M.W. Ackley, R.T. Yang, Kinetic separation by pressure swing adsorption: method of characteristics model, AIChE J. 36 (1990) 1229–1238.
[15] R.T. Yang, Gas Separation by Adsorption Processes, Butterworth Publishers, London, 1987.
[16] J.N. Kim, K.T. Chue, K.I. Kim, S.H. Cho, J.D. Kim, Non-isothermal adsorption of nitrogen–carbon dioxide mixture in a fixed bed of zeolite-X, J. Chem. Eng. Jpn. 27 (1994) 45–51.
[17] D.D. Do, Adsorption Analysis: Equilibria and Kinetics, Imperial College Press, London, 1998.
[18] K.T. Chue, J.N. Kim, Y.J. Yoo, S.H. Cho, R.T. Yang, Comparison of activated carbon and zeolite 13X for CO_2 recovery from flue gas by pressure swing adsorption, Ind. Eng. Chem. Res. 34 (1995) 591–598.
[19] S. Ergun, Fluid flow through packed columns, Chem. Eng. Prog. 48 (1952) 89–94.
[20] W. Yun, K.S. Lee, The use of cubic spline and far-side boundary condition for the collocation solution of a transient convection–diffusion problem, Korean J. Chem. Eng. 24 (2007) 204–208.
[21] S.Y. Choi, H.S. Kim, K.S. Lee, K.P. Yoo, W.H. Lee, Reduced-order distillation model using collocation method with cubic splines, Korean J. Chem. Eng. 8 (1991) 44–52.
[22] T.N.E. Greville, Theory and Applications of Spline Functions, Academic Press, New York, 1969.
[23] S.S. Suh, P.C. Wankat, Pressure swing adsorption process for binary gas separation with Langmuir isotherms, Chem. Eng. Sci. 44 (1989) 2407–2410.
[24] D. Kunii, J.M. Smith, Heat transfer characteristics of porous rocks, AIChE J. 6 (1960) 71–78.